Interface Behavior of Geogrid-Reinforced Sub-ballast: Laboratory and Discrete Element Modeling

Ngoc Trung Ngo and Buddhima Indraratna

Abstract This paper shows a study on the interface behavior of biaxial geogrids and sub-ballast using a direct shear box and computational modeling. A series of large-scale direct shear tests are performed on sub-ballast (capping layer) with and without geogrid inclusions. The laboratory test data indicate that the interface shear strength is mainly decided by applied normal stresses and types of geosynthetics tested. Discrete element modeling approach is used to investigate the interface shear behavior of the sub-ballast subjected to direct shear loads. Irregular-shaped sub-ballast particles are modeled by clumping of many spheres together in pre-determined sizes and positions. Biaxial geogrids are simulated in the DEM by bonding small balls together to build desired geogrid shapes and opening apertures. The numerical results reasonably match with the measured test data, showing that the introduced DEM model can simulate the interface behavior of sub-ballast stabilized by the geogrids. In addition, the triaxial geogrid presents the highest interface shear strength compared to the biaxial geogrids; and this can be associated with the symmetric geometry of grids' apertures that can distribute load in all directions. Evolutions of contact forces of unreinforced/reinforced sub-ballast specimens and contour strain distributions during shear tests are also investigated.

Keywords Transport geotechnics · Geogrid · Sub-ballast · Interface behavior · Discrete element method

N. T. Ngo (✉) · B. Indraratna
Faculty of Engineering and Information Sciences, Center for Geomechanics and Railway Engineering, University of Wollongong, Wollongong 2522, NSW, Australia
e-mail: trung@uow.edu.au

B. Indraratna
e-mail: indra@uow.edu.au

1 Introduction

With the rapid urbanization is ongoing across Australia, the need for appropriate ground improvement techniques is mandatory to build road and rail networks over soft subgrade having low shear strength. A typical ballasted track sub-structure commonly has a compacted layer of sub-ballast (capping layer) aving commonly broadly graded mixtures of sand and gravel placed above a subgrade. A ballast layer (i.e., 300–500 mm thick) placed over the sub-ballast (Selig and Waters 1994; Indraratna et al. 2011a). The typical functions of sub-ballast are to: (i) transmit and distribute the applied moving loads to the underneath layers at a decreased stress level (Powrie et al. 2007; Indraratna et al. 2013); (ii) to protect ballast particles from penetrating downward to the formation soil and to prevent subgrade fines from pumping up the upper ballast layer (Trani and Indraratna 2010); and (iii) to decrease the building up excess pore pressure under repeated train loads and to facilitate the drainage capacity of ballasted tracks (Indraratna et al. 2011a).During train operations, ballast aggregates become degraded and starts to lessen its shear strength and drainage capacity (Tutumluer et al. 2008; Rujikiatkamjorn et al. 2012; Ngo et al. 2017a, b, c), among others. Deterioration of track geometry due to excessive differential settlements and lateral displacements as a result of the localized failure of formations (sub-ballast and subgrade layers) often lead to the reduction in track stability and longevity. There have been an increasing use of planer geosynthetics (i.e., geogrids, geotextiles, or geo-composites) in ballasted tracks to decrease excessive settlements (differential settlements) and lateral deformations under dynamic train loading (Ngo and Indraratna 2016).

There have been numerous studies on soils stabilized by geosynthetics, but very few studies have been performed to investigate sub-ballast stabilized by geogrids using the experiment or via numerical modeling approaches (Ngo et al. 2016). In addition, these studies on sub-ballast were often limited by only using the continuum-modeling approach; and therefore, the discrete nature and angularly shaped particles of sub-ballast have not been modeled properly (Biabani et al. 2016; Indraratna et al. 2017), among others. It is found that these studies did not consider the possibility of using geogrids in reducing the thickness of the sub-ballast. Despite some attempts to study granular materials stabilized by geogrids, where the interaction mechanism and the interface responses between the sub-ballast(capping) and geogrid which is mainly governed by the interlocking among particles and geogrids are not modeled precisely in view of micro-mechanical aspects (Ngo et al. 2017a, b, c). In this paper, large-scale direct shear tests are performed, and discrete element method (DEM) is utilized to model geogrid-reinforced sub-ballast, investigating the shear stress–strain responses and corresponding contact force distributions of this composite assembly.

2 Laboratory Study

2.1 Large-Scale Direct Shear Test

A large-scale direct shear apparatus having typical dimension of 300 mm long 300 mm wide $\times$ 200 mm was used to investigate interface responses of the geogrid-stabilized sub-ballast, as illustrated in Fig. 1. The sub-ballast (capping) was collected from Bombo quarry, New South Wales, Australia. Prior to every test, ballast aggregates were cleaned and sieved, following to the Australian Standards, AS 2758.7 (1996). The particle size distribution characteristics of the sub-ballast tested in laboratory is identical to one often exercised in Australia (i.e., D_{max} = 19 mm, D_{min} = 0.075 mm, C_u = 16.3, C_c = 1.3, γ_d = 18.5 kN/m^3). Three different geogrids having varied shapes and opening apertures, as shown in Fig. 1, were used to study the influences of different types of geogrids' geometry on the shear strength of the composite specimens (Fig. 1).
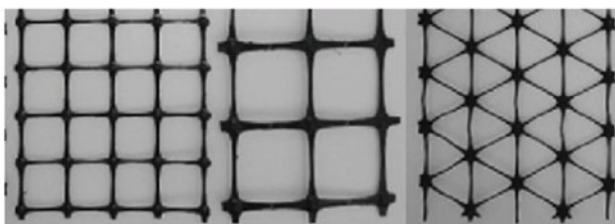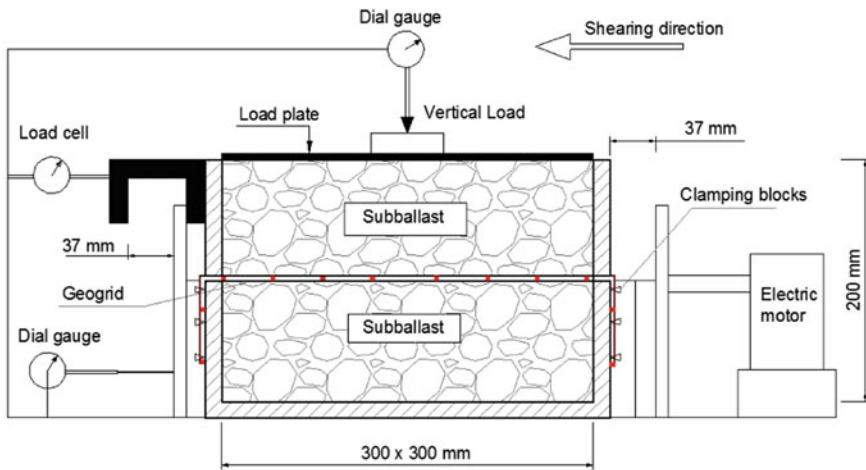
Fig. 1 Large-scale direct shear box and geogrids used

The sub-ballast was filled into the direct shear apparatus and compacted into every 100-mm-thick layer to attain an approximate field density of $\gamma_d = 18.5$ kN/m^3. A layer of geogrid was then embedded and secured at the middle of the upper and lower shear boxes. The upper part of the shear apparatus was then poured with remaining capping aggregates and compacted to the pre-determined density. It is noted that there is a small gap (around 1.5–2 mm) between the geogrid and the upper box so that the friction between them can be ignored during the shearing progress. A loading plate was sit on the top surface of the upper box and that allows the sub-ballast aggregates to move in vertical direction during shearing. This loading plate was also utilized to apply vertical normal loads to the ballast specimen and to record vertical displacements (i.e., normal strain) during the testing. Direct shear tests were sheared under low normal stresses of $\sigma_n = 6.7$–45 kPa, mimicking actual low confinements in real track conditions (Indraratna et al. 2013).The composite geogrid sub-ballast specimen was sheared to a given horizontal displacement of $\Delta h = 30$ mm ($\varepsilon_s = 10\%$). During shearing progress, shear forces, vertical, and horizontal displacements were recorded at every 1 mm of lateral displacements by a load transducer and displacement potentiometer, respectively.

3 Discrete Element Modeling

The discrete element method (DEM) was first introduced by Cundall and Strack (1979), and it has been increasingly adopted to study load-deformation responses of ballast particles (McDowell et al. 2006; Huang and Tutumluer 2011; Rujikiatkamjorn et al. 2013; Indraratna et al. 2014; Ngo et al. 2014; Ngo et al. 2017a, b, c), among others. Recently, the discrete element method (DEM) has been increasingly adopted in the recent past decades as promising alternatives to the continuum-based method for the study of granular materials. The DEM enables deeper insight into the micro-mechanical characteristics of granular materials such as contact force distributions, fabric anisotropy, and particle breakage that are almost impossible or unlikely to be measured in the laboratory (McDowell and Bolton 1998; O'Sullivan and Cui 2009; Huang et al. 2009b; Ngo et al. 2017a, b, c), among others.

3.1 Modeling Sub-Ballast Aggregates in DEM

Irregularly shaped sub-ballast particles having varied angularities (i.e., varying shapes and sizes) were simulated in the DEM by connecting and overlapping a number of spherical balls together at suitable positions (Ngo et al. 2017a, b, c). In this study, a library of nine sub-ballast particles was simulated by connecting 25–50 balls together, as illustrated in Fig. 2a. These simulated aggregates range from 2.5 to 19 mm and mimic the particle size distribution conducted experimentally. It is noted that small-sized particles were not used in these simulations is to reduce

required excessively calculation time. Ngo et al. (2014) and Lim and McDowell (2005) also adopted this approach to study the micro-mechanical behavior of granular materials, and they indicated that the absence of miniature aggregates has no significant affect on the results provided that the relative density of the specimen is identical as the one conducted in the laboratory.

The simulated sub-ballast particles were then placed inside the simulated shear box without any overlapping within the specified constrains of the simulated shear box and were further compacted to a given density of $\gamma_d = 18.5$ kN/m^3 that is identical to that conducted in the laboratory (Fig. 2b).

3.2 Modeling of Geogrids

Three types of geogrids were examined in the current analysis. Geogrids having different shapes and openings (i.e., apertures) was modeled by connecting a number of small balls together (i.e., balls having diameters of around 1.5–3 mm), as presented
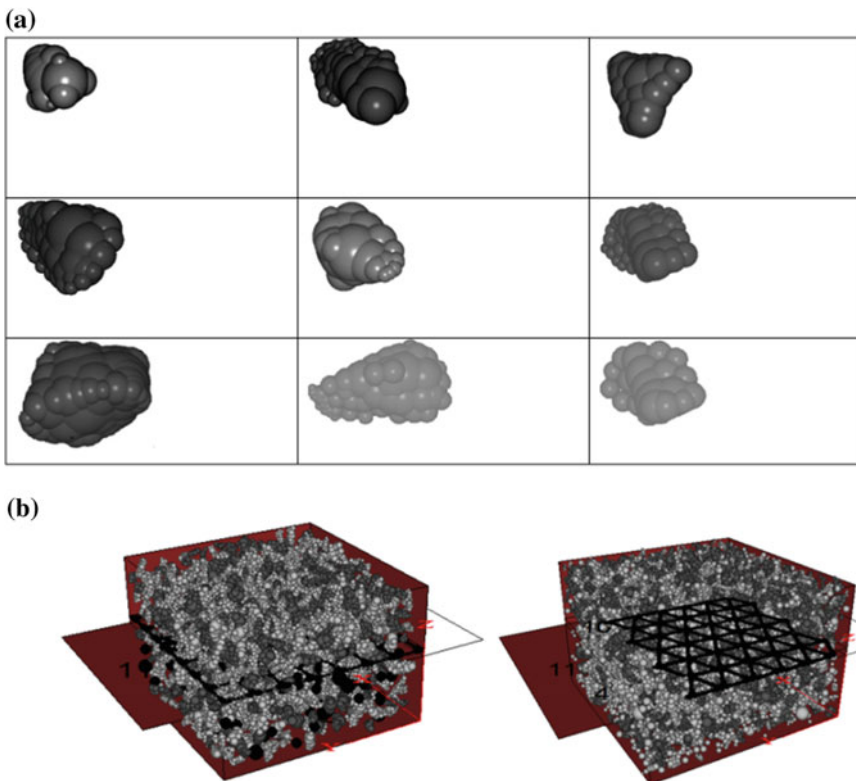

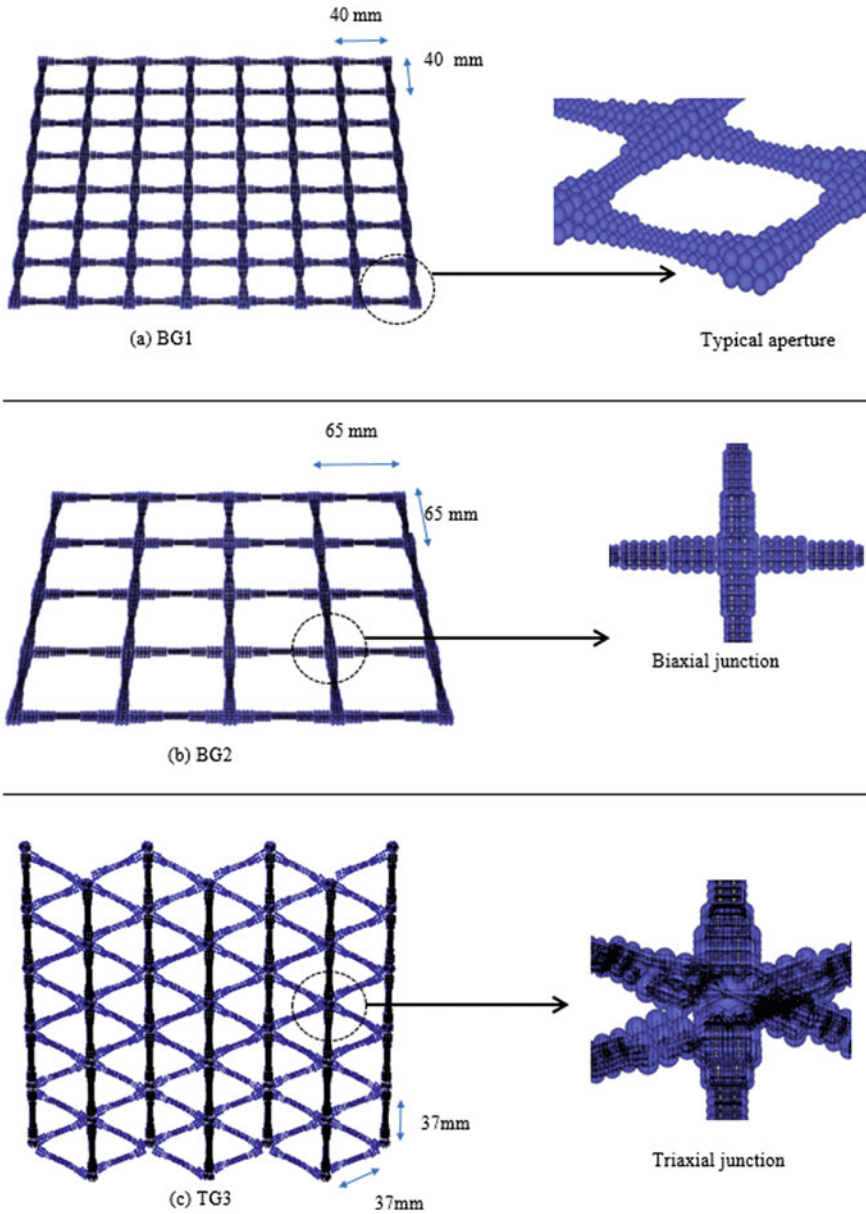Fig. 2 Modeling sub-ballast aggregates and shear box in DEM After Ngo et al. (2017a, b, c)

Fig. 3 Simulated geogrids in DEM: **a** Biaxial geogrid—BG1, 40 mm × 40 mm; **b** Biaxial geogrid—BG2, 65 mm × 65 mm; and **c** Triaxial geogrid—TG3 After Ngo et al. (2017a, b, c)

in Fig. 3. The geogrids comprise of spheres of varying sizes was modeled, where the bigger spheres were utilized to simulate the junctions of geogrids and the small spheres used for the middle of the geogrid ribs. Spheres were bonded together using
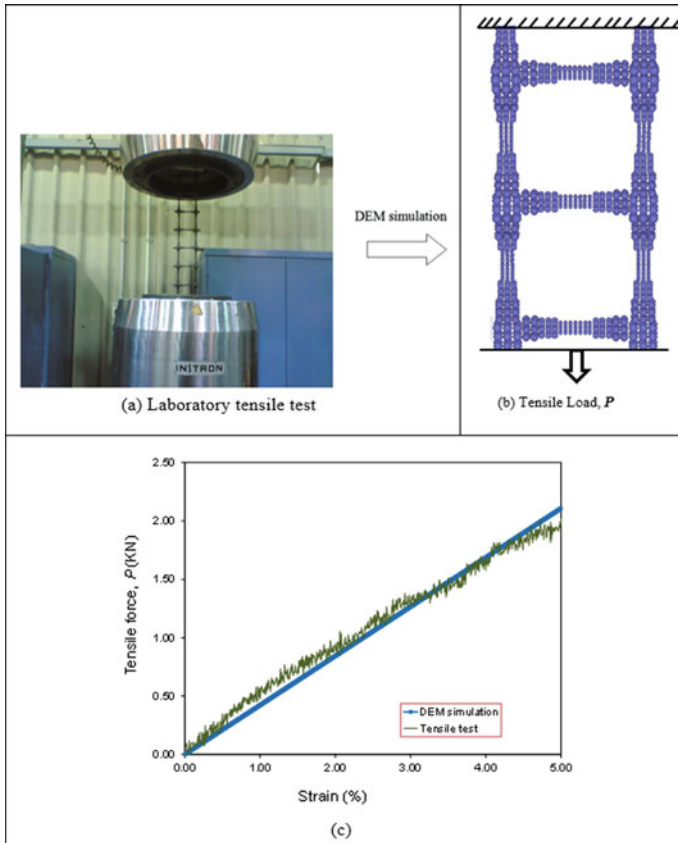
Fig. 4 **a** Tensile test for geogrids: **b** Predicted load-displacement from DEM; and **c** Comparison of DEM and laboratory test data *Data source* Ngo et al. (2017a, b, c)

parallel bonds corresponding to the measured tensile strength (i.e., within the geo-grid's elastic range of up to 5%) and were determined by calibrating with test data measured from tensile tests (Fig. 4). Each bond can represent the force–displacement responses of a finite-sized piece of cementation materials placed between two balls in contact and are able to carry both tensile forces and moments. Once the geogrid was generated and secured in the compacted sub-ballast, the model was cycled (i.e., iteration)to enable the simulated geogrid freely interact with the surrounding aggre-gates. Normal forces were applied to the loading plate of the shear box and were kept constantly by modifying the positions and displacements of the top plate via a servo-control mechanism developed by Itasca (2016). The composite assembly was then iterated to equilibrium state where a ratio of maximum un-balanced forces to the average contact forces was less than a set threshold of 1.15×10^{-4}. This condition applied to facilitate the interlock among sub-ballast aggregates and the geogrids and also enables the sub-ballast grains to build contacts with each other. This process also

ensured the unit weight (i.e., density) of the composite assembly unchanged. The shear box was then forced to shear horizontally at a speed of 8.35×10^{-5} mm/time step to a maximum lateral displacement of $\Delta h = 30$ mm.

3.3 Determination of Micro-Mechanical Parameters

Selecting the input micro-mechanical parameters (i.e., stiffness, parallel bond radius, parallel bond stiffness, etc.) can be complicated considering different parameters, i.e., stiffness k_n and k_s, friction coefficient f, and parameters for the bonding strength that governs the flexibility and tensile strength of geogrids. In this study, the input micro-mechanical parameters were selected by back-calculation of tensile load-displacement behavior with measured laboratory test data using an INSTRON tensile testing machine, as illustrated in Fig. 4. Simulations of tensile tests subject to varied normal and shear stiffness were then implemented. The tensile force–strain responses predicted from the DEM compared to those obtained in laboratory are presented in Fig. 4c. The calibration procedure was described elsewhere by Ngo et al. (2017a, b, c). Selected input parameters for simulating the geogrids and sub-ballast adopted in this study are presented in Table 1.

Input parameters of sub-ballast were also determined by calibrating the shear stress–strain behavior given by DEM modeling with those measured experimentally (Ngo et al. 2015; Biabani et al. 2016b). Contact stiffness (k_n, k_s) and inter-particle coefficient of friction (μ) to model sub-ballast were determined by direct shear tests of sub-ballast where these parameters were changed gradually until the predicted results agreed well with those measured in laboratory(i.e., similar technique used for the geogrids). It is noted that this approach is time-consuming and starting values of input parameters were selected from available literature. Figure 5 shows comparison of shear stress-displacement responses of sub-ballast with different values of μ; and it shows that when $\mu = 0.85$ exhibits a reasonable match with test data.

Table 1 Selected input parameters for geogrids and sub-ballast

Input parameters	Geogrid	Sub-ballast
Particle density (kg/m^3)	972	2350
Coefficient of friction	0.47	0.85
Contact normal stiffness, k_n (N/m)	5.91×106	4.82 E8
Contact shear stiffness, k_s (N/m)	5.91×106	2.41 E8
Contact normal stiffness of wall-particle, $k_{n\text{-wall}}$ (N/m)	3.25×109	3.25 E9
Shear stiffness of wall of wall-particle, $k_{s\text{-wall}}$ (N/m)	3.25×109	3.25 E9
normal strength, ϕ_n (kN)	56.8	
Parameters for contact bonds shear strength, ϕ_s (kN)	56.8	
Parallel bond radius multiplier	6.27 E7	
Parallel bond normal stiffness, k_{np} (kPa/m)	6.27 E7	
	0.5	
	297 E7	

Fig. 5 Influences of the friction coefficient, μ on the shear stress–strain behavior of sub-ballast
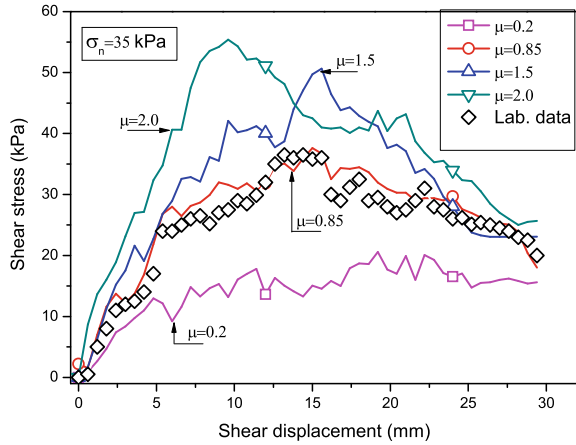
4 Results and Discussion

4.1 Shear Stress–Strain Responses

DEM modeling of large-scale shear tests for unreinforced sub-ballast were subjected to three different normal stresses of $\sigma_n = 6.7, 20.5$, and 45 kPa. The shear stress ratio (τ/σ_n) and the normal strain (ε_n) at a corresponding shear strain (ε_s) predicted by the DEM and compared with data measured in the laboratory are presented in Fig. 6. It is clearly seen that the DEM predictions match reasonably well with those measured experimentally under given normal stresses. The strain softening behavior of sub-ballast and its volumetric dilation were obtained in all DEM simulations; and it shows that the higher the normal stress (σ_n), the lower the shear stress ratio, τ/σ_n.

The introduced DEM model was then adopted to simulate sub-ballast reinforced by different geogrids (biaxial grids—BG1, BG2; and triaxial grid—TG3) subject to a low normal stress of 6.7 kPa, simulating small confinement in a real ballasted track. Figure 7 presents comparisons of the shear stress–strain responses predicted by DEM with those measured in the laboratory. It is observed that the predicted results agree well with the laboratory test data, implying that the proposed DEM model is able to predict the interface behavior of sub-ballast stabilized by the geogrids. The triaxial geogrid-reinforced sub-ballast shows the lowest volumetric dilation; and this is probably due to the symmetric geometry of the grid that can transfer the applied loads more uniformly and can also facilitate better interlock with the surrounding aggregates than the other types of geogrids. The enhanced performance provided by the triaxial grid (TG3) can also be associated with the isotropic-radial stiffness that is nearly constant in all direction, and that can restrain the sub-ballast particles better at their interfaces.
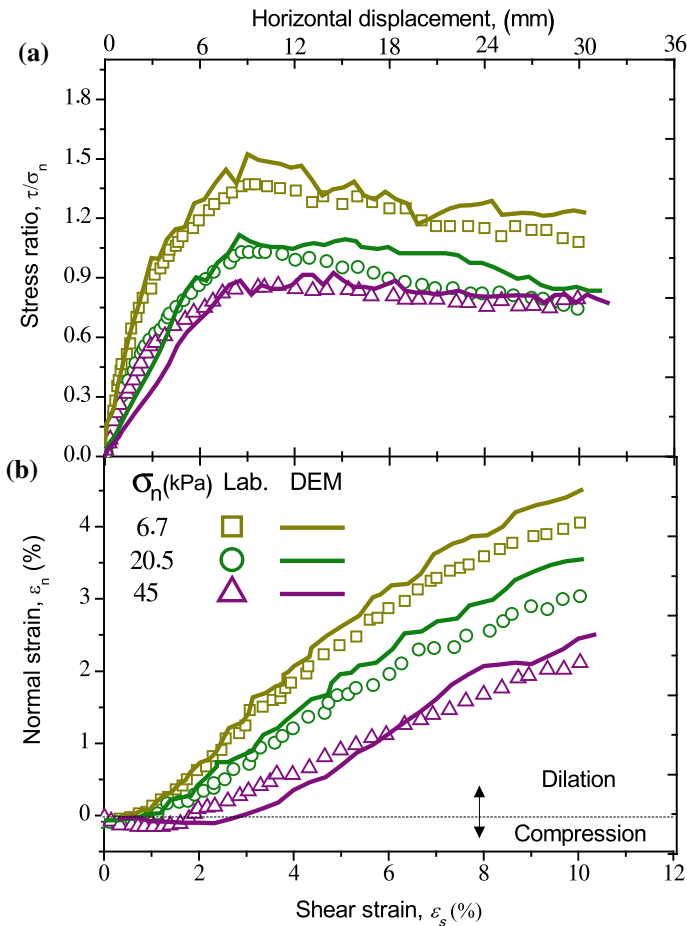
Fig. 6 a Shear stress ratio (τ/σ_n) plotted with shear strain, **b** normal strain plotted with shear strain *Data source* Ngo et al. (2017a, b, c)

4.2   Responses of the Geogrids

Figure 8 shows the distributions of mean contact forces plotted along the depth of the shear box for sub-ballast specimen sat a given shear strain of $\varepsilon_s = 5\%$ and a given normal stress of $\sigma_n = 6.7$ kPa. It is seen that the unreinforced sub-ballast shows the smallest induced contact forces compared to those for the reinforced specimens. The sub-ballast stabilized by the triaxial geogrid (TG3) exhibits the highest mobilized contact forces, approximately of 71 N (for TG3) compared to 53 and 39 N for biaxial grids BG1 and BG2, respectively. A confinement zone can be found in a depth of about 50 mm from the interface of geogrid and sub-ballast where the inclusion of geogrid results in a significant increase in induced contact
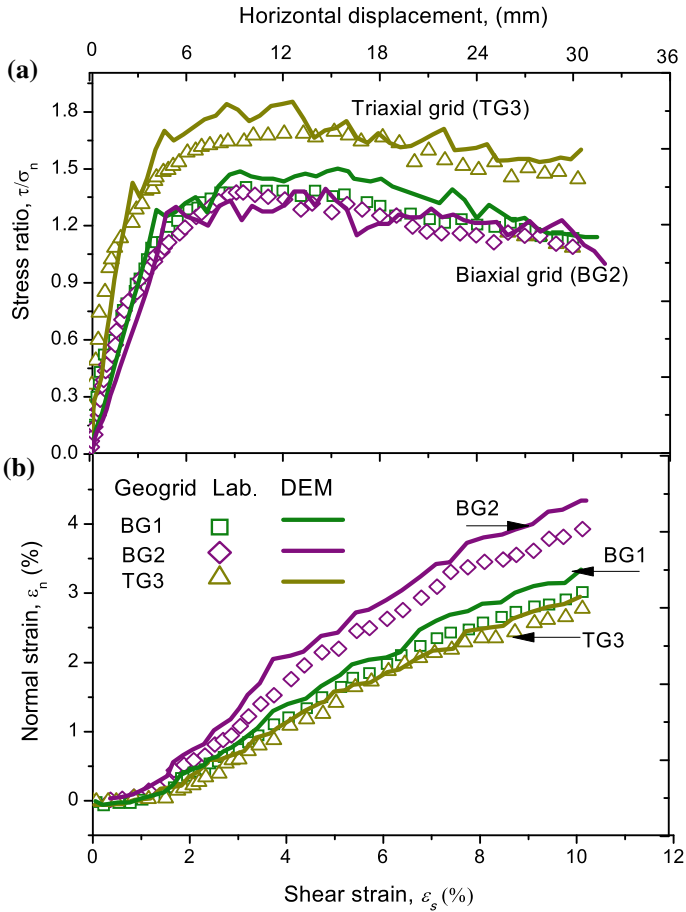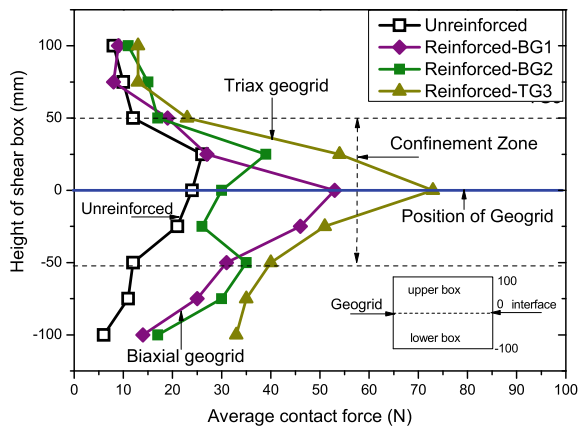
Fig. 7 **a** Shear stress ratio (τ/σ_n) plotted with shear strain, **b** normal strain plotted with shear strain After Ngo et al. (2017a, b, c)

Fig. 8 Mean contact forces of sub-ballast with and without geogrid subject to a shear strain of $\varepsilon_s = 5\%$

forces. The mean contact forces measured at the interface reach a value of approximately three times compared to those that are near to the top loading plate and bottom boundary of the shear box. This mobilization of large magnitude forces inside the confinement zone of grids was a result of the strong mechanical interlock occurred between them (e.g., Indraratna et al. 2011a; Ngo et al. 2014).

Figure 9 shows contour strains induces in the geogrids in lateral shearing direction (ε_{xx} measured at a given shear strain of $\varepsilon_s = 5\%$ (i.e., approximately measured at the peak shear strength) for a biaxial grid (BG1) and a triaxial grid (TG3). It is observed that strains develop non-uniformly across the geogrids where the mobilized strains may depend on the degree of interlock that occurs between the
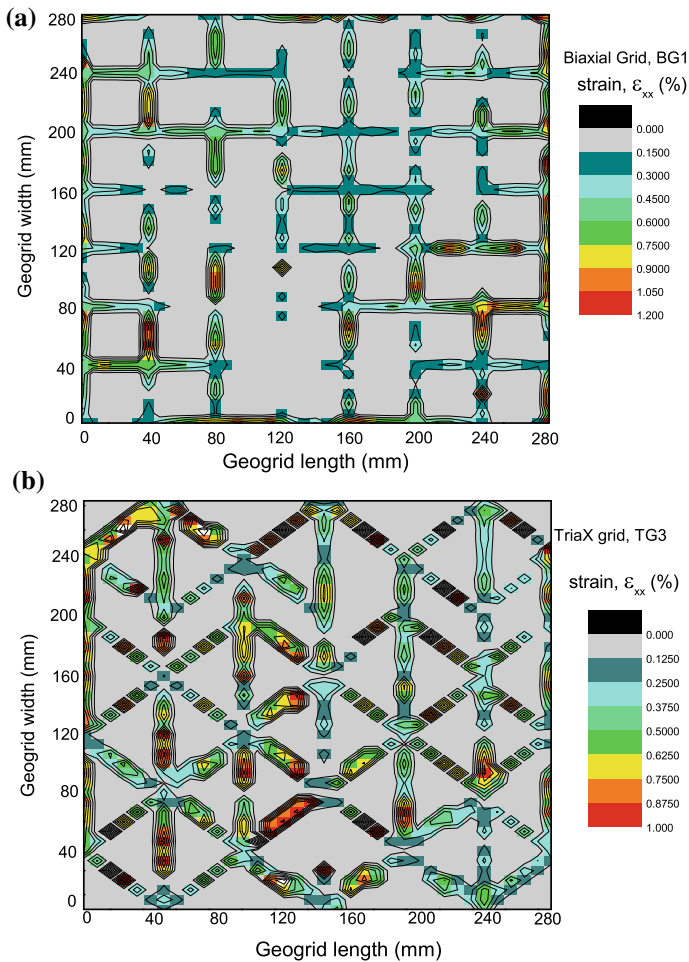

Fig. 9 Predicted contour strains induced across the geogrid: **a** Biaxial grid (BG1); and **b** Triaxial grid (TG3) *Data source* Ngo et al. (2017a, b, c)

geogrid and sub-ballast particles. It is noted that the triaxial grid (TG3) exhibits slightly smaller mobilized strains compared to the biaxial grid (BG1), approximately of 1.0% for the triaxial grid compared to 1.2% strain for biaxial grid, BG1. This can be justified by the symmetric shape of the triaxial grid that would provide better stress distribution than the square apertures.

5 Conclusions

Large-scale direct shear tests were performed on sub-ballast aggregates with and without the inclusion of different types of geogrid. The laboratory test results were used to calibrate and verify the proposed DEM models. DEM simulations for geogrids with varied shapes and opening apertures were simulated by connecting many spherical balls together.

The shear stress–strain responses predicted by the DEM analysis agreed well with experimental data, showing that the introduced DEM model can simulate the interface behavior of sub-ballast aggregates stabilized by different types of geogrids. Triaxial grid had the largest ratio of τ/σ_n while it exhibited the smallest volumetric dilation. This was due to the symmetrical shape of triangular apertures that can transfer applied loads across the geogrid and can provide a better interlock with granular particles. Taking advantages of DEM simulation, the variations of mean contact forces along the depth of the shear apparatus were presented for both unreinforced/reinforced sub-ballast specimens. The triaxial geogrid-stabilized sub-ballast experienced the largest mobilized contact forces at their interfaces. Contour strains mobilized across the geogrids in the lateral shearing direction were also analyzed.

References

AS 2758.7 (1996) Aggragates and rocks for engineering purposes; Part 7: Railway ballast, Sydney, NSW, Australia

Biabani MM, Indraratna B, Ngo NT (2016a) Modelling of geocell-reinforced subballast subjected to cyclic loading. Geotext Geomembr 44(4):489–503

Biabani MM, Ngo NT, Indraratna B (2016b) Performance evaluation of railway subballast stabilised with geocell based on pull-out testing. Geotext Geomembr 44(4):579–591

Cundall PA, Strack ODL (1979) A discrete numerical model for granular assemblies. Geotechnique 29(1):47–65

Huang H, Tutumluer E (2011) Discrete Element Modeling for fouled railroad ballast. Constr Build Mater 25:3306–3312

Huang H, Tutumluer E, Hashash YMA, Ghaboussi J (2009b) Discrete element modelling of aggregate behaviour in fouled railroad ballast. In: Geotechnical Special Publication, 192, pp 33–41

Indraratna B, Ngo NT, Rujikiatkamjorn C (2013) Deformation of coal fouled ballast stabilized with geogrid under cyclic load. J Geotech Geoenviron Eng 139(8):1275–1289

Indraratna B, Ngo NT, Rujikiatkamjorn C, Vinod J (2014) Behaviour of fresh and fouled railway ballast subjected to direct shear testing - a discrete element simulation. Int J Geomech ASCE 14 (1):34–44

Indraratna B, Salim W, Rujikiatkamjorn C (2011) Advanced rail geotechnology - ballasted track., CRC Press, Taylor & Francis Group, London, UK

Indraratna B, Sun Q, Ngo NT, Rujikiatkamjorn C (2017) Current research into ballasted rail tracks: model tests and their practical implications. Aust J Struct Eng 18(3):204–220

Itasca (2016) Particle flow code in three dimensions (PFC3D). Itasca Consulting Group Inc, Minnesota

Lim WL, McDowell GR (2005) Discrete element modelling of railway ballast. Granular Matter 7 (1):19–29

McDowell GR, Bolton M (1998) On the micromechanics of crushable aggregates. Geotechnique 48(5):667–679

McDowell GR, Harireche O, Konietzky H, Brown SF, Thom NH (2006) Discrete element modelling of geogrid-reinforced aggregates. Proc ICE - Geotech Eng 159(1):35–48

Ngo NT, Indraratna B (2016) Improved performance of rail track substructure using synthetic inclusions: experimental and numerical investigations. Int J Geosynthetics Ground Eng 2(3): 1–16

Ngo NT, Indraratna B, Rujikiatkamjorn C (2014) DEM simulation of the behaviour of geogrid stabilised ballast fouled with coal. Comput Geotech 55:224–231

Ngo NT, Indraratna B, Rujikiatkamjorn C (2015) A study of the behaviour of fresh and coal fouled ballast reinforced by geogrid using the discrete element method. In: Geomechanics from micro to macro - proceedings of the TC105 ISSMGE international symposium on geomechanics from micro to macro, IS-Cambridge 2014

Ngo NT, Indraratna B, Rujikiatkamjorn C (2016) Modelling geogrid-reinforced railway ballast using the discrete element method. Transport Geotech 8(2016):86–102

Ngo NT, Indraratna B, Rujikiatkamjorn C (2017a) Micromechanics-based investigation of fouled ballast using large-scale triaxial tests and discrete element modeling. J Geotech Geoenviron Eng 134 (2): pp 04016089

Ngo NT, Indraratna B, Rujikiatkamjorn C (2017b) Stabilisation of track substructure with geo-inclusions – experimental evidence and DEM simulation. Int J Rail Transport 5 (2): 63–86

Ngo NT, Indraratna B, Rujikiatkamjorn C (2017c) A study of the geogrid–subballast interface via experimental evaluation and discrete element modelling. Granular Matter 19 (3): 54, 51–16

O'Sullivan C, Cui L (2009) Micromechanics of granular material response during load reversals: combined DEM and experimental study. Powder Technol 193(3):289–302

Powrie W, Yang LA, Clayton CR (2007) Stress changes in the ground below ballasted railway track during train passage. In: Proceedings of the institution of mechanical engineers: part F: J of rail rapid transit, pp 247–261

Rujikiatkamjorn C, Indraratna B, Ngo NT, Coop M (2012) A laboratory study of railway ballast behaviour under various fouling degree. In: The 5th Asian regional conference on geosynthetics, pp 507–514

Rujikiatkamjorn C, Ngo NT, Indraratna B, Vinod J, Coop M (2013) Simulation of fresh and fouled ballast behavior using discrete element method. In: Proceedings of the international conference on ground improvement and ground control, pp 1585–1592. Singapore, Research Publishing

Selig ET, Waters JM (1994) Track geotechnology and substructure management. Thomas Telford, London

Trani LDO, Indraratna B (2010) Assessment of subballast filtration under cyclic loading. J Geotech Geoenviron Eng 136(11):1519–1528

Tutumluer E, Dombrow W, Huang H (2008) Laboratory characterization of coal dust fouled ballast behaviour. In: AREMA 2008 annual conference and exposition, Salt Lake City, UT, USA